



# Cobalt hydroxide nanoflakes intercalated into nitrogen-doped reduced graphene oxide's nanosheets for supercapattery application

Mehmood Shahid<sup>1</sup>, Arshid Numan<sup>2</sup>, Jayesh Cherusseri<sup>2,a)</sup> , Mohammad Khalid<sup>2</sup>, H. H. Somaily<sup>3,4</sup>, Chariya Kaewsaneha<sup>1,a)</sup>

<sup>1</sup> School of Integrated Science and Innovation, Sirindhorn International Institute of Technology (SIIT), Thammasat University, Pathum Thani 12121, Thailand

<sup>2</sup> Graphene & Advanced 2D Materials Research Group, School of Engineering and Technology, Sunway University, No. 5 Jalan Universiti, Bandar Sunway, 47500 Petaling Jaya, Selangor, Malaysia

<sup>3</sup> Research Center for Advanced Materials Science (RCAMS), King Khalid University, P.O. Box 9004, Abha 61413, Saudi Arabia

<sup>4</sup> Department of Physics, Faculty of Science, King Khalid University, P.O. Box 9004, Abha, Saudi Arabia

<sup>a)</sup> Address all correspondence to these authors. e-mails: drjayeshpuli@gmail.com; Chariya@siit.tu.ac.th

Received: 7 June 2022; accepted: 8 December 2022; published online: 9 January 2023

In this study, we report a one-step method to synthesize  $\text{Co}(\text{OH})_2$  nanoflakes intercalated into nitrogen-doped graphene oxide (NrGO). The NrGO- $\text{Co}(\text{OH})_2$  (abbreviated as NRCO) nanocomposite is used as a positrode to fabricate a supercapattery device with activated carbon as the negative electrode. The surface morphology and microstructure of the NRCO nanocomposites were confirmed by field emission scanning electron microscope imaging and the structure was analysed by X-ray diffraction and Raman spectroscopy. The electrochemical performances of the NRCO nanocomposite electrode are examined using cyclic voltammetry, electrochemical impedance spectroscopy, and galvanostatic charge/discharge measurement. The NRCO nanocomposite electrode displayed a specific capacity of 75.2 C/g in a 1 M KOH aqueous electrolyte. The cycle life of the supercapattery device fabricated with NRCO nanocomposite [with 2 wt.%  $\text{CO}(\text{OH})_2$ ] exhibits a specific capacity to retain 93.1% of its initial capacity even after completing 3000 continuous charge/discharge cycles, which shows its potential among current energy storage devices.

## Introduction

Ever-increasing energy crisis, environmental pollution, and increasing cost of petroleum-based fuels steer the direction of the current research toward renewable and sustainable energy resources such as solar and wind energy [1, 2]. The continuous supply of energy is vital in any case but sources such as solar and wind are not able to fulfill such criteria as they are intermittent in nature. To overcome the discrepancy of power fluctuation harvested from these sources, efficient energy storage systems are developed which can provide a continuous supply of power on demand regardless of the seasonal variations and day-night cycles. Batteries and supercapacitors are evolved as novel alternatives to the existing conventional electrochemical energy storage systems. They are meritorious among others in terms of their cost, efficiency and durability [3]. Metal-ion batteries such

as lithium-ion batteries and sodium-ion batteries are good in their energy density but lagging behind due to their low power density [4]. On the other hand, supercapacitors offer instantaneously high-power density, quick charge/discharge and durability for long-running applications and they are comparatively cheaper as well. These characteristics made supercapacitors to be an efficient electrochemical energy storage systems for the future [5].

The low energy density of supercapacitors makes them lag behind metal-ion batteries [6]. In order to increase their energy density and escalate them to make commercially viable candidates, various engineering strategies have been employed. Therefore, a new type of supercapacitor termed as 'hybrid supercapacitor' was designed that features both the characteristics of batteries and supercapacitors. But these hybrid supercapacitors

utilize electroactive materials, which are not capacitive in nature but they exhibit battery-like intercalated type charge storage. Hence, using the terminology hybrid supercapacitor is no longer valid and it creates a lot of confusion among the various energy storage mechanisms possible. Hence, these types of electrochemical energy storage devices are known as supercapatteries. They have combined features of batteries and supercapacitors in which they exhibit high energy densities like batteries and possess high-power density like supercapacitors [7]. In general, a supercapattery device makes use of a redox-active material as its positive electrode (termed as positrode), which is capable of providing high power and a carbonaceous material as a negative electrode (termed as negatrode) [8].

Among the various electrode-active materials, those exhibiting redox-type charge storage have been exploited as positrode materials including transition metal oxides, transition metal hydroxides and their nanocomposites with electronically conducting polymers. The oxides of transition metals are well explored due to their various oxidation states in ionic forms which alleviate oxidation reduction transitions and escalated charge storage process in the potential range of water decomposition [9, 10]. The nanostructures of transition metal oxides and hydroxides due to their excellent electrochemical properties are used in numerous applications such as sensors, electrocatalysis and supercapacitors. Although the most widely explored transition metal oxide is ruthenium oxide due to its excellent specific capacitance but due to its high cost and environmentally hazardous nature made it less popular [11]. Among the family of transition metal oxides and hydroxides, cobalt oxides and hydroxides have gained much attention of the researchers in the area of electrochemical energy storage systems due to their well-defined redox properties, high specific capacitance, peculiar physio-chemical properties and low cost [12, 13]. The nanostructures of cobalt oxides/hydroxides are diverse in their morphologies and are investigated widely in the field of energy storage systems [5]. The aggregation phenomena in nanostructures of metal oxides/hydroxides is a major drawback in electrochemical storage applications which affects the efficiency of the materials by decreasing their electroactive sites, and structural changes that occur within the electrode during the course of charge–discharge cycles. Therefore, preparing nanocomposites with electronically conducting fillers becomes a viable option to overcome these issues. Carbon nanomaterials are much preferred as conducting filler materials as they exhibit good electronic conductivity, good mechanical strength, good chemical, thermal stabilities, etc. Hence, preparing nanocomposites of transition metal oxides and/or hydroxides with carbon nanomaterials is an effective strategy.

In the library of carbonaceous materials, a 2D nanomaterial, graphene possesses unique characteristics such as high mechanical strength, good electronic conductivity, high mechanical

strength, large specific surface area, wide electrochemical potential window, etc. [14, 15]. The various functional groups such as epoxide and hydroxyl can increase the heterogeneous charge transfer rate on the graphene surface [16]. Its efficiency of charge transportation could be effectively increased if doped with suitable elements like nitrogen which ultimately increases its electrochemical performance. As graphene exhibits high electronic conductivity hence introducing nitrogen as a hetero-atom in between the layers of 2D graphene may lead to an enhancement in electronic conductivity as well as its electrochemical activity [17]. So, a combination of cobalt hydroxide (CO) with novel hierarchical nitrogen-doped graphene helps in disaggregating the nanostructures of cobalt hydroxide. The nitrogen-doped graphene also facilitates charge transfer, whereas electroactive sites of cobalt hydroxide contribute to the oxidation and reduction reactions thereby boosting the electrochemical performance.

In the present study, we report the synthesis and characterizations of nitrogen-doped reduced graphene oxide (NrGO)/Co(OH)<sub>2</sub> (herein abbreviated as NRCO) nanoflake hybrids and their use as positrode in supercapatteries. This is the first-time report on using NRCO hybrids for supercapattery applications. Combining NrGO with Co(OH)<sub>2</sub> helps in blocking the possible aggregation issue of Co(OH)<sub>2</sub> nanoflakes and the charge storage can be further improved due to the synergistic effect of these two materials. The NrGO facilitates charge transfer within the NRCO hybrid electrode as well as imparts stability, whereas the redox-active Co(OH)<sub>2</sub> contributes to the enhanced charge storage. The NRCO hybrid electrode exhibits a maximum specific capacity of 75.2 C/g in 1 M KOH aqueous electrolyte, which is higher than pristine Co(OH)<sub>2</sub> nanoflake positrode (60.1 C/g) and NRCO-4 (64.5 C/g) and NRCO-8 (53.2 C/g). We have fabricated a supercapattery using NRCO as positrode and activated carbon (AC) as negatrode. The assembled hybrid supercapattery device exhibits remarkable electrochemical performances when compared to its individual counter-parts. The NRCO//AC supercapattery device delivered an energy density of 18.54 Wh/kg and a power density of 435.8 W/kg at a current density of 2.5 A/g. The NRCO//AC supercapattery device exhibited a specific capacity retention of 3000 cycles. The present work proclaims the use of NRCO hybrid electrodes for future generation supercapatteries.

## Results and discussion

### X-ray diffraction

The crystallinity and phase identification was performed by XRD. Figure 1(a) depicts the XRD spectrum of pristine Co(OH)<sub>2</sub> nanoflakes. Sharp and well-defined peaks positioned at  $2\theta = 19.1^\circ, 32.4^\circ, 38^\circ, 51^\circ, 58.1^\circ, 61.4^\circ$  and  $69.7^\circ$  correspond to the (001), (010), (011), (012), (110), (111) and (103) lattice

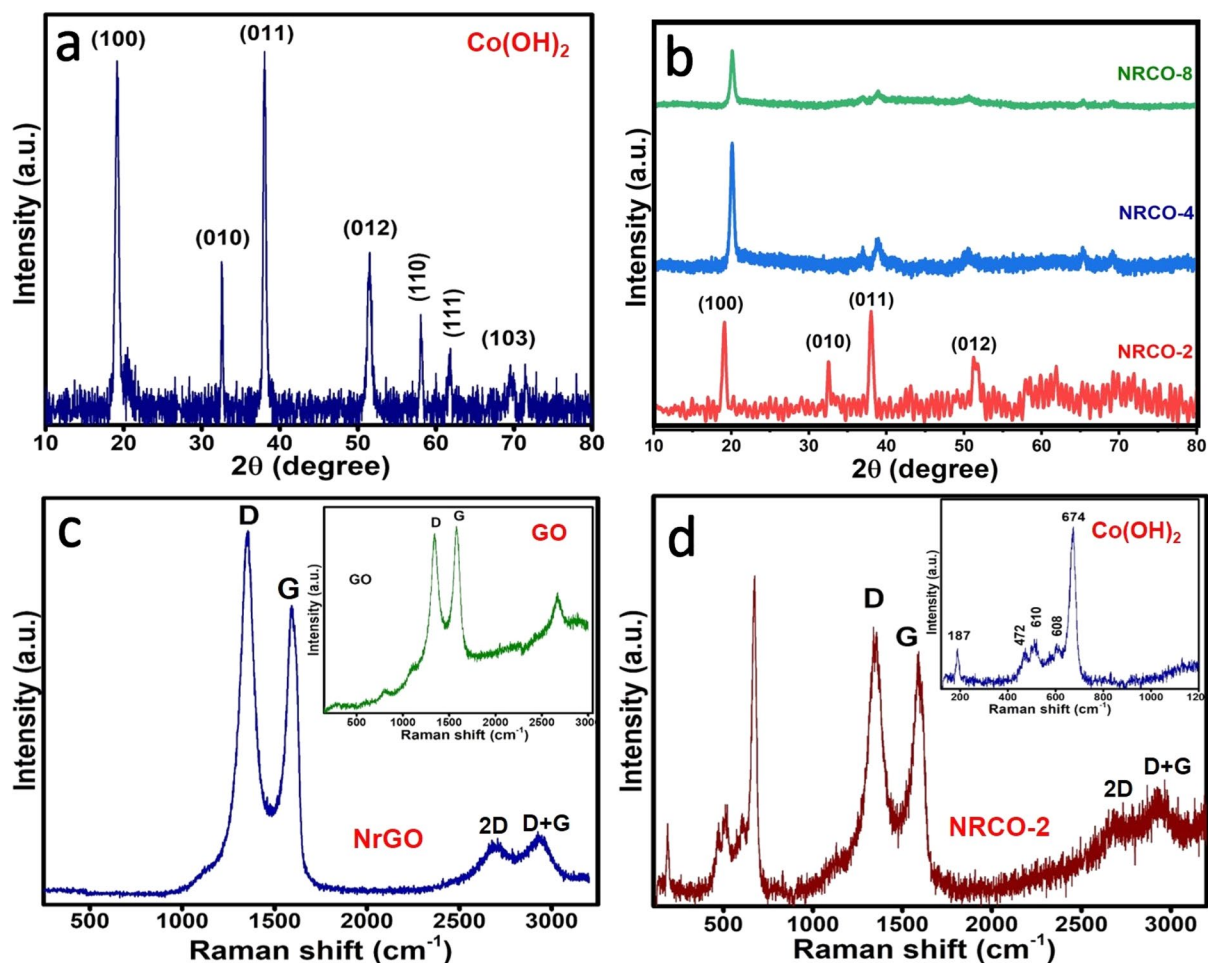


**Figure 1:** XRD spectrum of (a) pristine  $\text{Co(OH)}_2$  nanoflakes, (b) NRCO-2, NRCO-4 and NRCO-8 nanocomposites; Raman spectrum of (c) NrGO (Inset: Raman spectrum of GO) and (d) NRCO-2 nanocomposite (Inset: Raman spectrum of pristine  $\text{Co(OH)}_2$  nanoflakes).

planes of  $\text{Co(OH)}_2$ . All these characteristic peaks correspond to the hexagonal structure of  $\text{Co(OH)}_2$  (JCPDS 96–101-0268). A similar spectrum with all the designated peaks with the low intensity mentioned above was also observed for the NRGO nanocomposite samples shown in Fig. 1(b) too. It is found that by increasing the contents of NrGO, peak intensities of  $\text{Co(OH)}_2$  were decreased systematically. This is due to the integration of  $\text{Co(OH)}_2$  flakes on the NrGO nanosheets which lead to less exposure of  $\text{Co(OH)}_2$  flakes. XRD results are also supported by FESEM images in which  $\text{Co(OH)}_2$  flakes can be sandwiched at higher contents of NrGO, and it is explained in the next part of this discussion. The decrease in intensity and more broadening of the peaks can be observed in the case of NRCO-2 nanocomposite samples, which is attributed to the intercalation of  $\text{Co(OH)}_2$  nanoflakes on NrGO nanosheets. Moreover, no other peaks were notified in the case of NRGO nanocomposite samples, which reveals the successful synthesis of NRGO nanocomposites.

### Raman spectroscopy

Raman spectroscopy is the most conventional and non-destructive technique in determining the functional group moieties and structural defects produced in graphite and graphene-based nanomaterials [18]. The Raman spectrum of NrGO is shown in Fig. 1(c) and the corresponding Raman spectrum of the GO is given in the inset. Very prominent and sharp peaks corresponding to the graphitic band (G-band) and defect band (D-band) are located at  $1596$  and  $1354 \text{ cm}^{-1}$  for both GO and NrGO. The D-band is associated with the lattice defects in the GO and NrGO, whereas G-band renders the vibration of  $\text{sp}^2$  bonds of C–C in the honeycomb structure of GO and NrGO [5]. The ratio between the D-band intensity ( $I_D$ ) to G-band intensity ( $I_G$ ) (termed as ' $I_D/I_G$ ') is important to determine the degree of reduction of GO. The  $I_D/I_G$  ratio is found to be 0.98, which increased to 1.25 for NrGO upon reduction. This manifests the reduction in  $\text{sp}^2$

domains and the removal of functional groups [19]. In the case of NRCO-2 nanocomposite, the  $I_D/I_G$  ratio reduced to 1.06 when compared to pristine NrGO, which may be due to the reduction of domain size of  $sp^2$  and transformation of  $sp^3$  to  $sp^2$  [5]. Additionally,  $\text{Co}(\text{OH})_2$  nanoflakes get intercalated during their growth which eventually acts as a spacer material between the nanosheets of graphene. Another sharp peak can be observed in the pristine GO spectra (2D band) located at  $2685\text{ cm}^{-1}$ , which is attributed to the second-order phonon vibrations [20]. But this peak got suppressed with a much broader peak in the case of NrGO sample due to the reduction of GO nanosheets and formation of more confinement. After the reduction process, apart from this 2D band, there exists another peak for the NrGO sample ((D + G)-band), located at  $2949\text{ cm}^{-1}$  (red-shift of graphitic disorder), which is attributed to the reduction of GO in to smaller sheets [21]. These 2D and (D + G) peaks can be observed in the case of NRCO-2 nanocomposite but with noise due to the incorporation of  $\text{Co}(\text{OH})_2$  between the layers of graphene nanosheets hence cannot be distinguished properly. The Raman spectrum of pristine  $\text{Co}(\text{OH})_2$  is shown in the inset of Fig. 1(d). From this spectrum, it can be seen that prominent peaks observed at 187 and 472 are corresponding to O–Co–O bending. The peaks located at 510, 608 and  $674\text{ cm}^{-1}$  correspond to CoO (Ag) symmetric stretching and CoO (A1g) symmetric stretching mode of  $\text{Co}(\text{OH})_2$ , respectively [22].

### Morphological characterization and elemental mapping

The surface morphology and microstructure of the samples are examined using FESEM imaging. The FESEM images of pristine  $\text{Co}(\text{OH})_2$  nanoflakes, pristine NrGO nanosheets and NRCO nanocomposites (NRCO-2, NRCO-4 and NRCO-8) are shown in Fig. 2. Figure 2(a) and (b) represents the FESEM images of pristine NrGO nanosheets at two different magnifications. The NrGO exhibited a layered architecture with wrinkled morphology. These nanosheets exhibit large surface area which is beneficial for the successful formation of NRCO nanocomposite with  $\text{Co}(\text{OH})_2$  nanoflakes. These nanosheets can act as spacer material which can avoid any possible agglomeration of individual  $\text{Co}(\text{OH})_2$  nanoflakes otherwise. Figure 2(c) depicts the FESEM image of pristine  $\text{Co}(\text{OH})_2$  nanoflakes. They are found to be circular in shape and of uniform shape and size in the order of 300–350 nm, which were aggregated together. The reason for this aggregation arises from the synthesis procedure in which the individual  $\text{Co}(\text{OH})_2$  nanoflakes were grown in the solution simultaneously during the hydrothermal reaction. However, this aggregation of  $\text{Co}(\text{OH})_2$  nanoflakes was significantly reduced when 2 wt.% NrGO was added to prepare the NRCO-2 nanocomposite, which is shown in Fig. 2(d). In fact, the oxygen containing electronegative functional groups on NrGO sheets acted as the nucleation sites for  $\text{Co}(\text{OH})_2$  nanoflakes thereby avoiding any independent solution phase growth that might have resulted in reducing the chances for the aggregation of

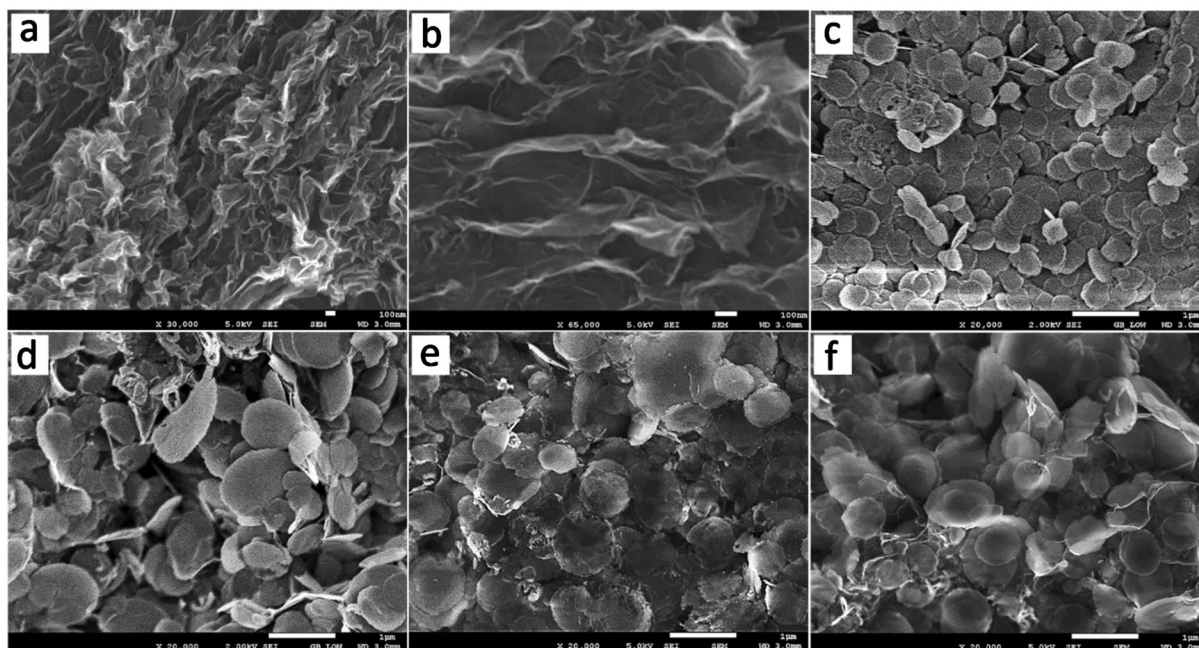


**Figure 2:** FESEM images of (a and b) pristine NrGO nanosheets at different magnifications, (c) pristine  $\text{Co}(\text{OH})_2$  nanoflakes, (d) NRCO-2 nanocomposite, (e) NRCO-4 nanocomposite and (f) NRCO-8 nanocomposite.

Co(OH)<sub>2</sub> nanoflakes. As the weight of NrGO was increased from 2 to 4 wt% (in the case of NRCO-4 nanocomposite), the Co(OH)<sub>2</sub> nanoflakes got intercalated in the NrGO nanosheets irregularly which affected the formation of agglomerates for a large extent as shown in Fig. 2(e). But as the weight of NrGO was increased from 4 to 8 wt.% (in the case of NRCO-8 nanocomposite), the Co(OH)<sub>2</sub> nanoflakes once again agglomerated each other and the nanosheets separated from the Co(OH)<sub>2</sub> nanoflakes [Fig. 2(f)] due to improper intercalation, since the concentration becomes very high for an optimal intercalation to happen.

We have examined the electrochemical performances of the pristine Co(OH)<sub>2</sub> and the NRCO nanocomposites (this is discussed next section of this article) and found that the NRCO-2 nanocomposite performs better in terms of specific capacity and cycle life. This made us to select the optimal electrode composition to be used as a positrode in fabricating the supercapattery to be NRCO-2. To estimate the elemental distribution within the NRCO-2 nanocomposite, EDS elemental mapping analysis was performed. Figure 3 demonstrates the EDS elemental mapping of NRCO-2 nanocomposite. Figure 3(a) shows the FESEM image which is used in the EDS elemental mapping. Figure 3(b) shows the EDS spectrum received for the NRCO-2 nanocomposite. The EDS spectrum of NRCO-2 nanocomposite exhibits prominent peaks corresponding to cobalt, oxygen, carbon and nitrogen and no peaks corresponding to other elements represent the purity of the sample synthesized. The EDS elemental mapping images for carbon, cobalt, oxygen, and nitrogen are shown in Fig. 3(c), (d), (e) and (f), respectively. individual elemental distribution of carbon, cobalt, oxygen and nitrogen is shown in Fig. 3(c–f). A high density of green, red and grey dots represents an increased concentration of carbon, cobalt and oxygen, respectively. However, a few blue dots representing nitrogen

reveal that the doping concentration is very low. The EDS elemental mapping demonstrates the homogenous distribution of all elements and the formation of NRCO-2 nanocomposite.

## Electrochemical performances

### Three-electrode cell studies

The electrochemical performances of all the samples were investigated by EIS, CV and GCD measurement. Figure 4 shows the CV curves of pristine Co(OH)<sub>2</sub> nanoflakes-based electrode, and the NRCO nanocomposite electrodes performed at different scan rates in 1 M KOH aqueous electrolyte kept at 25 °C. The scan rates opted for the testing were 3, 5, 10, 20, 30, 40 and 50 mV/s. Figure 4(a) represents the CV curves of pristine Co(OH)<sub>2</sub> nanoflakes-based electrode, the nature of CV curves depicts the charge storage is of redox type as with prominent reduction and oxidation peaks. The same nature can also be seen in the case of NRCO-2 nanocomposite electrode [Fig. 4(b)], NRCO-4 nanocomposite electrode [Fig. 4(c)] and NRCO-8 nanocomposite electrode [Fig. 4(d)]. Among the nanocomposite electrodes, a high current density was achieved for the NRCO-2 nanocomposite electrode. This can be due to the optimal concentration of Co(OH)<sub>2</sub> and NrGO that makes an uniform distribution in the nanocomposite to make a hierarchical electrode nanostructure. If the individual components in a nanocomposite electrode get aggregated, the electrochemical performance gets decreased due to the low utilization of the specific surface area of the nanocomposite electrode architecture. All the NRCO nanocomposite electrodes exhibit well-defined redox peaks, which arise due to the diffusion of electrolyte ions towards the inner pores of the electrode nanostructure and the redox reactions to occur, the same for any battery material [23]. When the scan rate is increased, the oxidation and reduction peaks of all the

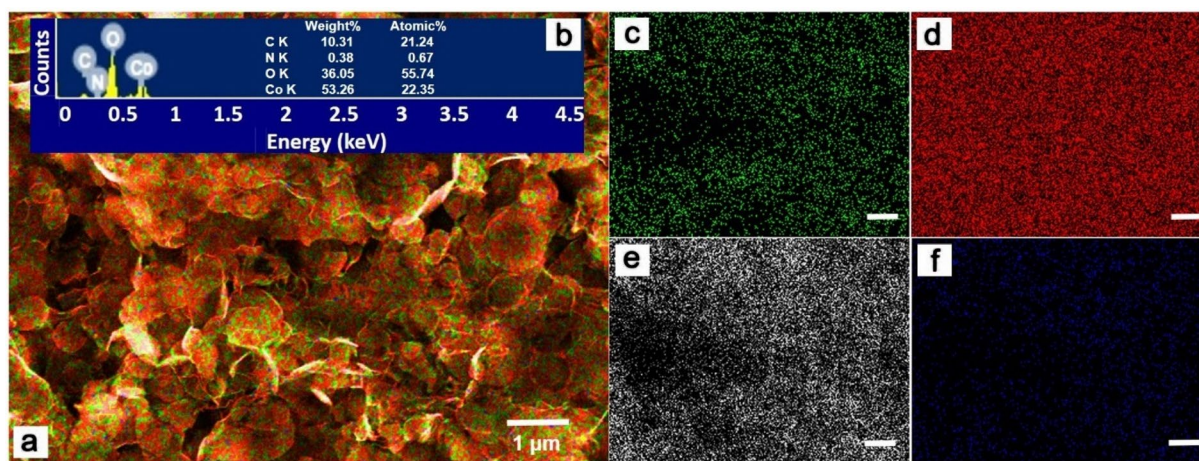


**Figure 3:** (a) FESEM image of NRCO-2 nanocomposite; (b) EDS spectrum of NRCO-2 nanocomposite with quantity information; (c–f) EDS elemental mapping images (scale bar: 500 nm) for (c) carbon, (d) cobalt, (e) oxygen and (f) nitrogen.

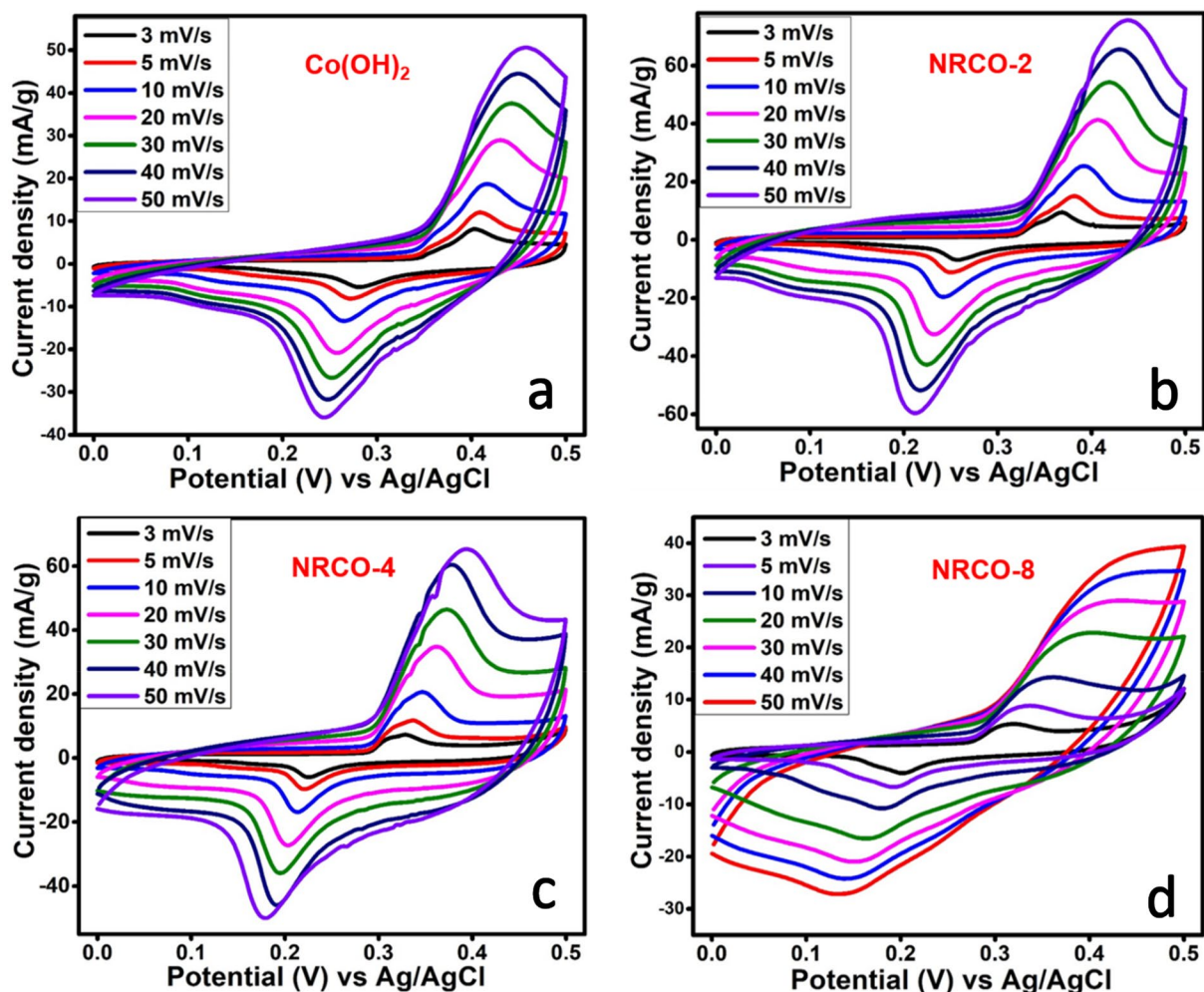


**Figure 4:** CV curves of electrodes made of (a)  $\text{Co(OH)}_2$  nanoflakes, (b) NRCO-2, (c) NRCO-4 and (d) NRCO-8 nanocomposites in 1 M KOH aqueous electrolyte.

nanocomposite electrodes got shifted toward lower and higher potentials, respectively. This is mainly due to the internal resistance played inside the nanostructured electrode which eventually hinders the movement of charges. At higher scan rates, the charge flow cannot follow the potential sweep which leads to a shift in redox potential [24]. It is evident from Fig. 4 that for all the NRCO nanocomposite electrodes, the redox potentials got shifted left with the increase in the scan rate. The redox reactions at all the electrodes can be represented by the following chemical equation [25]:



A comparison of CV curves of all the NRCO nanocomposite electrodes is shown in Fig. 5(a). The reduction potential for  $\text{Co(OH)}_2$  nanoflakes-based electrode is 0.4 V. However, the redox peak current got significantly improved in the cases

of NRCO-2 and NRCO-4 nanocomposite electrodes. A slight decrease in the oxidation peak potential can be observed at 0.36 and 0.33 V for NRCO-2 and NRCO-4 nanocomposite electrodes, respectively. The enhancement in the peak current and potential is due to the incorporation of NrGO nanosheets, which significantly reduces the aggregation of individual nanoflakes leading to the opening up of more pores and an enhanced redox reaction is expected due to the active interaction of electrolyte ions with the electrode-active material. However, the redox peak current got decreased significantly in the case of NRCO-8 nanocomposite electrode when compared to that of NRCO-2 and NRCO-4 nanocomposite electrodes. This is mainly due to the agglomeration of  $\text{Co(OH)}_2$  nanoflakes within the NRCO nanocomposite, which is evident from the FESEM images discussed previously. Hence, there is an optimal concentration of  $\text{Co(OH)}_2$  nanoflakes in NrGO sheets and in our case it was 2 wt%. The enhanced performance of NRCO-2 nanocomposite is due to the synergistic

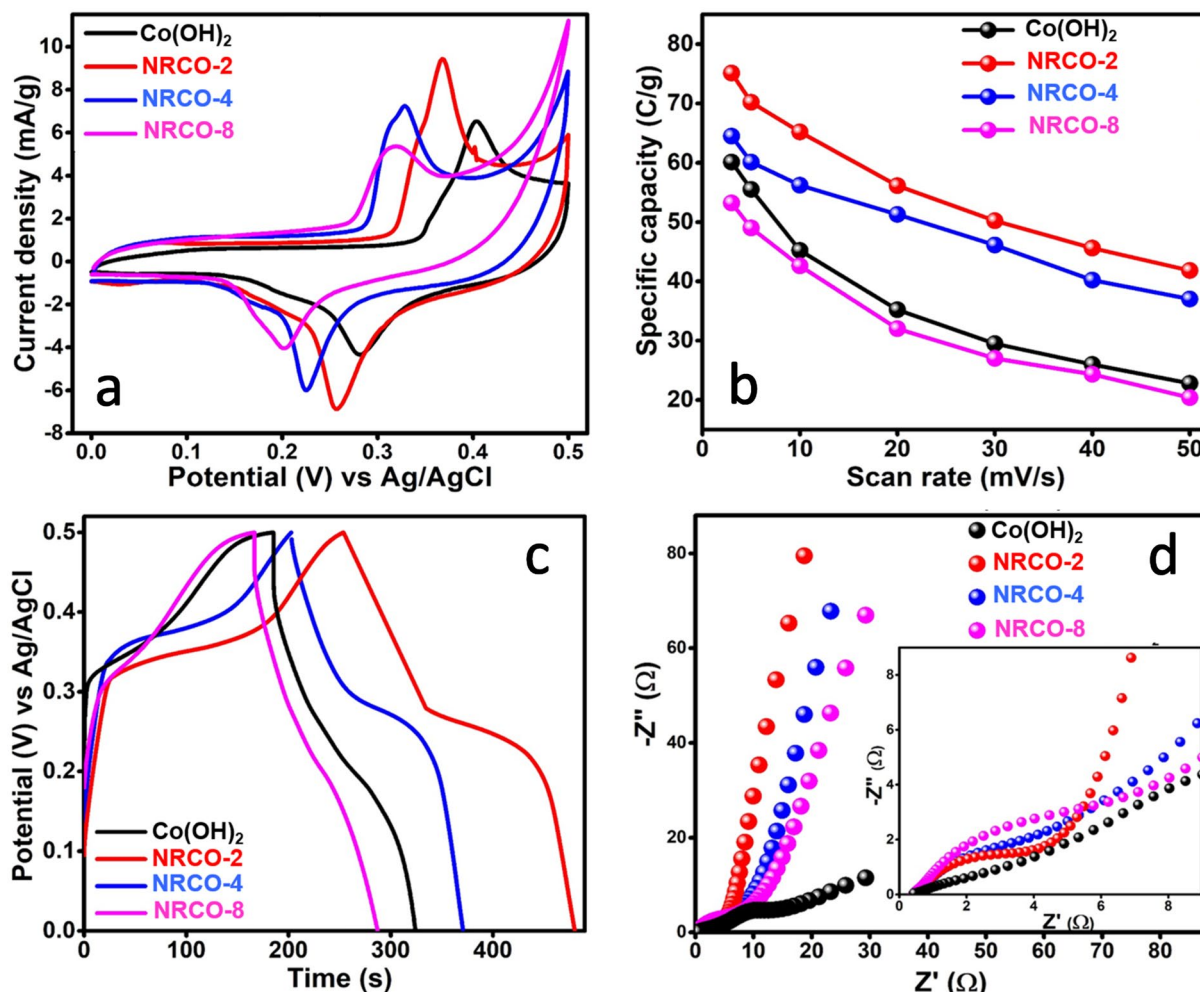


**Figure 5:** (a) Comparative CV curves of pristine  $\text{Co(OH)}_2$ -based electrode and NRCO nanocomposite electrodes; (b) Specific capacity exhibited by pristine  $\text{Co(OH)}_2$ -based electrode and NRCO nanocomposite electrodes at different scan rates; (c) comparative GCD curves of pristine  $\text{Co(OH)}_2$ -based electrode and NRCO nanocomposite electrodes; and (e) Nyquist plots of pristine  $\text{Co(OH)}_2$ -based electrode and NRCO nanocomposite electrodes.

effect of individual components which take part in the electrochemical performance of the supercapattery electrodes.

Overall, the NRCO-2 nanocomposite presented the best electrochemical performance with high specific capacity. The specific capacity ( $Q_s$ ) of the nanocomposite is calculated from the CV curve using the equation [26]

$$Q_s = \frac{1}{vm\Delta} \int_{V_i}^{V_f} I \times V dV, \quad (2)$$

where integral term provides the area under each CV curve,  $V$  is the potential window,  $v$  is the scan rate (in V/s),  $I$  is the current and  $m$  is the mass loading (g) of the electrode-active material. The specific capacity for the pristine  $\text{Co(OH)}_2$  nanoflakes-based electrode and NRCO nanocomposite electrodes obtained at different scan rates were calculated and plotted in Fig. 5(b). The specific capacity obtained for the pristine  $\text{Co(OH)}_2$  nanoflakes-based electrode was only 60.1, whereas it was found to be higher

for the NRCO nanocomposite electrodes. The highest specific capacity was observed for the NRCO-2 nanocomposite (75.2 C/g), whereas it was only 64.5 and 53.2 for the NRCO-4 and NRCO-8 nanocomposite electrodes, respectively. The specific capacity got decreased with an increase in the scan rate due to the decrease in kinetics. At a high scan rate of 50 mV/s, the specific capacities obtained are 22.8, 41.7, 37 and 20.4 C/g for pristine  $\text{Co(OH)}_2$ -based electrode, NRCO-2, NRCO-4, and NRCO-8 nanocomposite electrodes, respectively.

Figure 5(c) displays the comparative GCD curves of pristine  $\text{Co(OH)}_2$ -based electrodes and NRCO nanocomposite electrodes obtained at a constant current density of 400 mA/g. All the electrodes demonstrated non-linear GCD curves, which is due to the battery-type charge storage characteristics [8, 27]. Among all electrodes, the NRCO-2 nanocomposite electrode exhibited better performance when compared to other electrodes. The longest discharge curve was obtained for the

NRCO-2 nanocomposite electrode, which reveals its high potential in electrochemical energy storage as it can hold charges for a longer duration. EIS is an effective tool for investigating the inherent resistances of the electrode, electrolyte, electrode/electrode interfaces, etc. [28]. Figure 5(d) shows the Nyquist plots of the pristine  $\text{Co}(\text{OH})_2$ -based electrode and NRCO nanocomposite electrodes. The Nyquist plots of all these electrodes consist of three distinguishable regions: (i) a semicircle at high-frequency region, denotes the resistances arises from the electrodes, connection wires, current collector, etc., (ii) a Warburg line with a slope of  $\sim 45^\circ$  at high-medium frequency region, represents the combined effect of resistive and capacitive components within the electrode system, (iii) a vertical straight-line at the low-frequency region represents the pure capacitive-type charge storage possessed by the electrode system [23]. An enlarged view of the Nyquist plot at the high-frequency region is provided as an inset image in Fig. 5(d). The bulk electrolyte resistance ( $R_b$ ) is the total resistance offered by the supercapattery.  $R_b$  can be measured from the Nyquist plot using manual graphical approach by measuring the intersection point of the semicircle with the and X-axis.  $R_b$  is inversely proportional to the conductivity of electrode-active materials and it is an indirect method of understanding the conductivity of the electrodes. We have calculated the  $R_b$  of  $\text{Co}(\text{OH})_2$  nanoflakes-based electrode and NRCO nanocomposite electrodes by manual graphical approach. The  $R_b$  values of 16.8, 5.2, 6.1 and 7.5  $\Omega$  are obtained for the  $\text{Co}(\text{OH})_2$  nanoflakes-based electrode, NRCO-2, NRCO-4 and NRCO-8 nanocomposite electrodes. From this it can be said that the pristine  $\text{Co}(\text{OH})_2$  nanoflakes-based electrode exhibits high bulk electrolyte resistance, possibly due to the agglomeration of individual  $\text{Co}(\text{OH})_2$  nanoflakes within the electrode. The NRCO nanocomposite electrodes exhibit smaller semicircles (indicates low  $R_b$ ) when compared to that of the pristine  $\text{Co}(\text{OH})_2$  nanoflakes-based electrode, which reveals their good conductivity and better charge transfer kinetics. The reduction in the resistance of the electrodes is mainly due to the addition of NrGO with the  $\text{Co}(\text{OH})_2$  nanoflakes so that their conductivity gets increased as a result of the synergistic effect. The enhanced electrochemical performance due to the low  $R_b$  is evident from the CV and GCD measurements too. The NrGO plays an important role in decreasing the  $R_b$  of the electrodes by serving as a spacer material between the individual  $\text{Co}(\text{OH})_2$  nanoflakes, and an enhanced electron transport was achieved.

### Supercapattery device testing

We have fabricated a supercapattery device using NRCO-2 nanocomposite electrode as a positrode and AC electrode as a negatrode. The reason why we selected the NRCO-2 as a positrode is that it showed the best electrochemical performance among other two nanocomposite electrodes. The potential

window for NRCO-2//AC supercapattery device was selected from 0 to 1.5 V, where the potential window was carefully selected by estimating the proper working potential windows of each electrode in three-electrode cell configurations [3]. Figure 6(a) depicts the CV curves of the as-fabricated NRCO-2//AC supercapattery device obtained at different scan rates in 1 M KOH aqueous electrolyte. The shape of the CV curve was well maintained at all scan rates. The nature of the CV curve at higher scan rates remains the same as at lower scan rates which signify the good electrochemical stability of the supercapattery device. Although the redox peaks are not prominent at high scan rates but can be clearly seen from the lower scan rates, say 80 mV/s and lower. The prominent redox peaks that appeared on the CV curves validate the battery-like charge storage exhibited by the NRCO nanocomposite electrodes. Figure 6(b) depicts the GCD curves of the supercapattery device obtained at different current densities varied from 0.6 to 2.6 A/g. A maximum specific capacity of 91.2 C/g was obtained for the NRCO-2//AC supercapattery device calculated at a current density of 0.6 A/g. The specific capacity got reduced to 60 C/g when the current density was increased to 2.5 A/g. In order to evaluate the energy density (in Wh/kg) and power density (in W/kg) of the NRCO-2//AC supercapattery device, the following equations [29] are used:

$$E = \frac{\Delta V \times Q_s}{2 \times 3.6} \quad (3)$$

$$P = \frac{E \times 3600}{\Delta t} \quad (4)$$

where  $\Delta V$  is the discharge potential calculated by subtracting the voltage (IR) drop,  $\Delta t$  is the discharge time and  $Q_s$  is the specific capacity calculated from discharge curves.

A maximum energy density of 18.5 Wh/kg at a power density of 435.8 W/kg was obtained at a current density of 0.6 A/g for the NRCO-2//AC supercapattery device. The energy density got reduced to 3.4 Wh/kg with a significant increase in power density value to 540 W/kg when calculated at a current density of 2.5 A/g. EIS was also employed to understand the charge transfer mechanisms in the NRCO-2//AC supercapattery device. The Nyquist plot of the NRCO-2//AC supercapattery device is shown in Fig. 6(c). This supercapattery device displayed a low charge transfer resistance of 12  $\Omega$ . For commercial applications, the cycle of any electrochemical energy storage device is an important factor. A schematic diagram showing the assembly of the NRCO-2//AC supercapattery device is given as an inset image in Fig. 6(c). In order to estimate the electrochemical behaviour of the NRCO-2//AC supercapattery device at different cycle numbers, GCD measurement was carried out for continuous 3000 cycles at a constant current density of 2 A/g. The capacity increased for the initial number of cycles, say for the first 300 cycles, it was



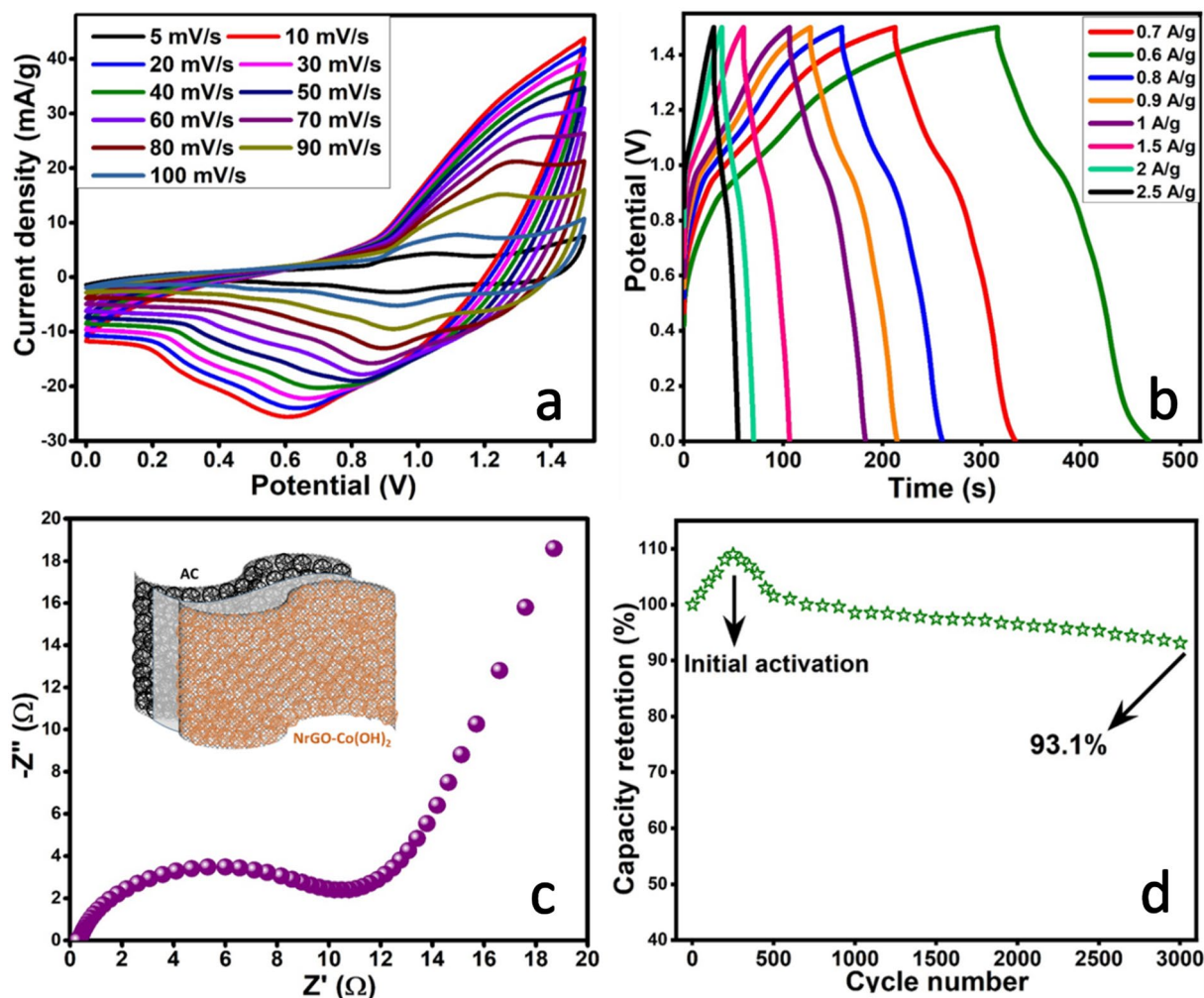
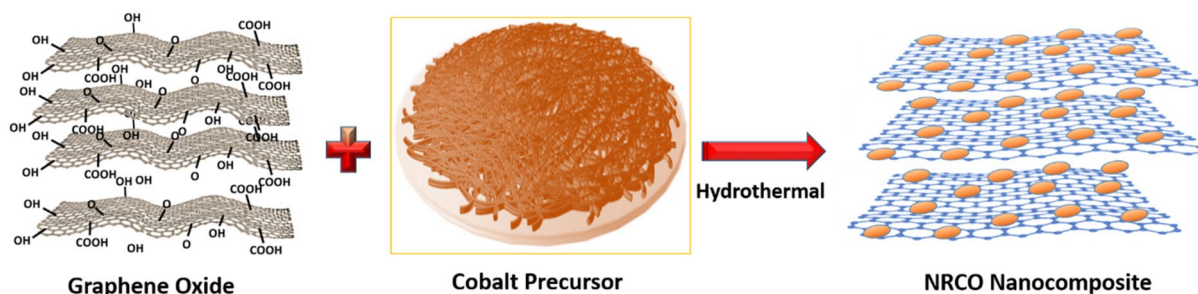


**Figure 6:** (a) CV curves of NRGO-2//AC supercapattery device obtained at different scan rates; (b) GCD curves of NRGO-2//AC supercapattery device obtained at different current densities; (c) Nyquist plot of NRGO-2//AC supercapattery and (d) life cycle test of NrGO-Co(OH)<sub>2</sub>//AC supercapattery.

due to the initial activation process that occurred within the electrode-active material. The synchronization of electrolyte ions with the electrode-active materials happens only after the electrolyte ions are accessible to the electrode-active materials' surface, which triggers the redox reaction. The movement of electrolyte ions through the porous structures of the nanocomposite is time-dependent and voltage-driven hence the activation step leads to an enhancement in the actual performance of any electrochemical energy storage device such as supercapacitor [30]. But immediately after 300 charge/discharge cycles, the performance started to degrade and reached 100% of its initial capacity after 500 cycles and was constant for the next 500 or cycles. The specific capacity decreased in a rhythmic manner from 100 to 95% after 2000 charge/discharge cycles. A capacity retention of 93.1% was obtained for the NRGO-2//AC supercapattery device even after 3000 charge/discharge cycles, which demonstrates its excellent durability for long-running applications.

### Conclusions

In this work, we successfully synthesized hierarchical nanocomposites consisting of NrGO and Co(OH)<sub>2</sub> by a facile one-step hydrothermal method. The pristine materials and nanocomposites were characterized by versatile tools such as XRD, Raman spectroscopy, FESEM imaging, and EDS. The successful synthesis of NRGO nanocomposites was confirmed using these analyses. The electrochemical energy storage performances of the NRGO nanocomposite electrodes were tested and the NRGO-2 nanocomposite electrode exhibited better performance when compared to other electrodes. The enhanced performance obtained for the NRGO-2 nanocomposite electrode was due to the synergistic effect of both NrGO nanosheets and Co(OH)<sub>2</sub> nanoflakes that gives an optimal concentration for the nanocomposite formation. The NRGO nanocomposite electrode displayed a specific capacity of 75.2 C/g in 1 M KOH aqueous electrolyte. An asymmetric supercapattery device was also fabricated using NRGO-2 as positrode and AC as negatrode using 1 M



**Scheme 1:** Schematic diagram showing the facile synthesis of NRCO nanocomposite.

KOH aqueous electrolyte. The performance of the NRCO-2//AC supercapattery device was examined using EIS, CV and GCD measurements that showed excellent performance. A maximum specific capacity of 91.2 C/g was obtained for the supercapattery device at a current density of 0.6 A/g. A maximum energy density of 18.5 Wh/kg at a power density of 435.8 W/kg at a current density of 0.6 A/g was achieved for the device. The cycle life of the supercapattery device was also tested and found to retain 93.1% of its initial capacity even after 3000 continuous charge/discharge cycles.

## Materials and methods

### Materials

In order to prepare graphene, graphite flakes were bought from Asbury Inc. (USA). Sulphuric acid ( $\text{H}_2\text{SO}_4$ , 98%), phosphoric acid ( $\text{H}_3\text{PO}_4$ , 98%), hydrochloric acid (HCl, 35%), hydrogen peroxide ( $\text{H}_2\text{O}_2$ ) and ammonia solution ( $\text{NH}_3$ , 25%) and N-Methyl-2-pyrrolidone (NMP) were obtained from Merck. Potassium permanganate ( $\text{KMnO}_4$ , > 99%), Cobalt acetate tetrahydrate [ $\text{Co}(\text{CH}_3\text{COO})_2 \cdot 4\text{H}_2\text{O}$ ], hydrazine hydrate ( $\text{N}_2\text{H}_4 \cdot \text{H}_2\text{O}$ , 50–60%), active carbon (AC), polyvinylidene fluoride (PVDF) and acetylene black were purchased from Sigma-Aldrich, Malaysia.

### Synthesis of NRCO hybrids

The synthesis of NRCO is reported by a method reported in the literature [14]. In a typical synthesis procedure, 1 mmol of  $\text{Co}(\text{CH}_3\text{COO})_2 \cdot 4\text{H}_2\text{O}$  is dissolved in 10 mL of DI water. This solution was added dropwise in 2 wt. % of graphene oxide (GO) solution under constant stirring. The rGO was prepared by a simplified hummers method [31]. The above mixture was stirred for 1 h to allow  $\text{Co}^{2+}$  to interact with the electronegative functional groups. A 13 mL of ammonia water (6%) was added to the mixture and stirred for the next 15 min. Subsequently, 2 mL of  $\text{N}_2\text{H}_4$  solution was added to mixture which is then transferred into 100 mL of Teflon-lined stainless-steel autoclave at 180 °C for 12 h. The precipitate was collected and

washed via ultracentrifugation with a copious amount of DI water and dried at 60 °C in a vacuum oven for 12 h thereafter. The sample was labelled as NRCO-2. The same procedure was opted to prepare the samples with different weight percentages of GO such as 4 and 8 wt.%, which were labelled as NRCO-4 and NRCO-8, respectively. The  $\text{Co}(\text{OH})_2$  nanoflakes were prepared in the same manner. Scheme 1 represents the facile preparation of NRCO nanocomposite using NrGO nanosheets and  $\text{Co}(\text{OH})_2$  nanoflakes.

### Material characterizations

The surface morphology and microstructural examinations are carried out by field emission scanning electron microscope (FESEM) imaging [FESEM JEOL JSM-7600F fitted with electron X-ray spectroscope (EDS)]. The elemental distribution with thin the supercapattery electrodes was examined using EDS. The structure of samples was characterized by X-ray diffraction (XRD) [Philips X'per X-ray diffractometer with  $\text{K}\alpha$  radiation ( $\lambda = 1.5418$  nm) at a scan rate of  $0.02$  deg  $\text{s}^{-1}$ ]. In order to examine the defects and degree of reduction of GO, Raman spectroscopy was employed [Renishaw inVia™ 2000,  $\lambda = 514$  nm].

### Fabrication of electrodes and supercapattery

The supercapattery electrodes were prepared using 75 wt.% of NRCO-2, 15 wt.% of AC and polymer binder (PVDF, 10 wt.%) were mixed in NMP to obtain a uniform slurry. This slurry was then coated on a pre-cleaned nickel foam (of geometrical area  $1$   $\text{cm}^2$ ) and dried at 80 °C for 12 h thereafter. The average mass loading of electroactive material (NRCO-2) was 5 mg. The same procedure was adopted to prepare the pristine  $\text{Co}(\text{OH})_2$  nanoflake electrode, NRCO-4 nanocomposite electrode and NRCO-8 nanocomposite electrode.

### Electrochemical characterizations

All the electrochemical measurements were recorded at room temperature (25 °C) using 1 M KOH aqueous electrolyte. Standard three-electrode cell measurements were performed using

electroactive material coated with nickel foam, platinum wire and Ag/AgCl as working, counter and reference electrodes, respectively. Electrochemical impedance spectroscopy (EIS) was used to examine the role of interfacial references at the electrode/electrolyte system. Cyclic voltammetry (CV) analysis was carried out to estimate the charge storage characteristics of the electrodes and supercapattery device. Galvanostatic charge/discharge (GCD) measurement was employed to understand the charge/discharge behaviour of the supercapattery device. All the electrochemical characterizations are carried out using a potentiostat-galvanostat, Gamry Interface1000 Instrument, USA.

## Acknowledgments

This work was supported by King Khalid University through a grant (KKU/RCAMS/22) under the Research Center for Advanced Materials Science (RCAMS) at King Khalid University, Saudi Arabia. This study was also supported by Thammasat Post-doctoral Fellowship, Thammasat University, Thailand.

## Funding

Funding was provided by Research Center for Advanced Materials Science, King Khalid University (KKU/RCAMS/22) and Sirindhorn International Institute of Technology, Thammasat University.

## Data availability

The data used to support the finding of this study are included in the article.

## Declarations

**Conflict of interest** The authors declare no conflict of interest.

## References

- I. Dincer, Renewable energy and sustainable development: a crucial review. *Renew. Sustain. Energy Rev.* **4**(2), 157–175 (2000)
- A. Akella, R. Saini, M.P. Sharma, Social, economical and environmental impacts of renewable energy systems. *Renew. Energy* **34**(2), 390–396 (2009)
- J. Iqbal, A. Numan, S. Rafique, R. Jafer, S. Mohamad, K. Ramesh, S. Ramesh, High performance supercapattery incorporating ternary nanocomposite of multiwalled carbon nanotubes decorated with  $\text{Co}_3\text{O}_4$  nanograins and silver nanoparticles as electrode material. *Electrochim. Acta* **278**, 72–82 (2018)
- V. Etacheri, R. Marom, R. Elazari, G. Salitra, D. Aurbach, Challenges in the development of advanced Li-ion batteries: a review. *Energy Environ. Sci.* **4**(9), 3243–3262 (2011)
- A. Numan, N. Duraisamy, F.S. Omar, Y. Mahipal, K. Ramesh, S. Ramesh, Enhanced electrochemical performance of cobalt oxide nanocube intercalated reduced graphene oxide for supercapacitor application. *RSC Adv.* **6**(41), 34894–34902 (2016)
- N. Duraisamy, A. Numan, S.O. Fatin, K. Ramesh, S. Ramesh, Facile sonochemical synthesis of nanostructured NiO with different particle sizes and its electrochemical properties for supercapacitor application. *J. Colloid Interface Sci.* **471**, 136–144 (2016)
- I. Heng, C.W. Lai, J.C. Juan, A. Numan, J. Iqbal, E.Y.L. Teo, Low-temperature synthesis of  $\text{TiO}_2$  nanocrystals for high performance electrochemical supercapacitors. *Ceram. Int.* (2018).
- G.Z. Chen, Supercapacitor and supercapattery as emerging electrochemical energy stores. *Int. Mater. Rev.* **62**(4), 173–202 (2017)
- W. Guoping, Z. Lei, Z. Jiujun, A review of electrode materials for electrochemical supercapacitors. *Chem. Soc. Rev.* **41**, 797–828 (2012)
- N.S. Choi, Z. Chen, S.A. Freunberger, X. Ji, Y.K. Sun, K. Amine, G. Yushin, L.F. Nazar, J. Cho, P.G. Bruce, Challenges facing lithium batteries and electrical double-layer capacitors. *Angew. Chem. Int. Ed.* **51**(40), 9994–10024 (2012)
- C.-C. Hu, K.-H. Chang, M.-C. Lin, Y.-T. Wu, Design and tailoring of the nanotubular arrayed architecture of hydrous  $\text{RuO}_2$  for next generation supercapacitors. *Nano Lett.* **6**(12), 2690–2695 (2006)
- C. Yuan, L. Hou, L. Shen, D. Li, F. Zhang, C. Fan, J. Li, X. Zhang, A novel method to synthesize whisker-like  $\text{Co}(\text{OH})_2$  and its electrochemical properties as an electrochemical capacitor electrode. *Electrochim. Acta* **56**(1), 115–121 (2010)
- X.-H. Xia, J.-P. Tu, X.-L. Wang, C.-D. Gu, X.-B. Zhao, Mesoporous  $\text{Co}_3\text{O}_4$  monolayer hollow-sphere array as electrochemical pseudocapacitor material. *Chem. Commun.* **47**(20), 5786–5788 (2011)
- M.M. Shahid, P. Rameshkumar, A. Pandikumar, H.N. Lim, Y.H. Ng, N.M. Huang, An electrochemical sensing platform based on a reduced graphene oxide–cobalt oxide nanocube@ platinum nanocomposite for nitric oxide detection. *J. Mater. Chem. A* **3**(27), 14458–14468 (2015)
- V. Chabot, D. Higgins, A. Yu, X. Xiao, Z. Chen, J. Zhang, A review of graphene and graphene oxide sponge: material synthesis and applications to energy and the environment. *Energy Environ. Sci.* **7**(5), 1564–1596 (2014)
- H. Chang, H. Wu, Graphene-based nanocomposites: preparation, functionalization, and energy and environmental applications. *Energy Environ. Sci.* **6**(12), 3483 (2013)
- A. Pandikumar, G.T.S. How, T.P. See, F.S. Omar, S. Jayabal, K.Z. Kamali, N. Yusoff, A. Jamil, R. Ramaraj, S.A. John, Graphene and its nanocomposite material based electrochemical sensor platform for dopamine. *RSC Adv.* **4**(108), 63296–63323 (2014)
- A. Numan, M.M. Shahid, F.S. Omar, S. Rafique, S. Bashir, K. Ramesh, S. Ramesh, Binary nanocomposite based on  $\text{Co}_3\text{O}_4$

- nanocubes and multiwalled carbon nanotubes as an ultrasensitive platform for amperometric determination of dopamine. *Microchim. Acta* **184**(8), 2739–2748 (2017)
19. A. Numan, M.M. Shahid, F.S. Omar, K. Ramesh, S. Ramesh, Facile fabrication of cobalt oxide nanograin-decorated reduced graphene oxide composite as ultrasensitive platform for dopamine detection. *Sens. Actuators B* **238**, 1043–1051 (2017)
  20. R. Yadav, C.J.J.O.S.A.M. Dixit, Devices, synthesis, characterization and prospective applications of nitrogen-doped graphene: a short review. *J. Sci.* **2**(2), 141–149 (2017).
  21. G. Witjaksono, M. Junaid, M.H. Khir, Z. Ullah, N. Tansu, M.S.B.M. Saheed, M.A. Siddiqui, S.S. Ba-Hashwan, A.S. Algamili, S.A.J.M. Magsi, Effect of nitrogen doping on the optical bandgap and electrical conductivity of nitrogen-doped reduced graphene oxide. *Molecules* **26**(21), 6424 (2021)
  22. U.M. Patil, R.V. Ghorpade, M.S. Nam, A.C. Nalawade, S. Lee, H. Han, S.C. Jun, PolyHIPE derived freestanding 3D carbon foam for cobalt hydroxide nanorods based high performance supercapacitor. *Sci. Rep.* **6**, 35490 (2016)
  23. F.S. Omar, A. Numan, S. Bashir, N. Duraisamy, R. Vikneswaran, Y.-L. Loo, K. Ramesh, S. Ramesh, Enhancing rate capability of amorphous nickel phosphate supercapattery electrode via composition with crystalline silver phosphate. *Electrochim. Acta* **273**, 216–228 (2018)
  24. F.S. Omar, A. Numan, N. Duraisamy, S. Bashir, K. Ramesh, S. Ramesh, A promising binary nanocomposite of zinc cobaltite intercalated with polyaniline for supercapacitor and hydrazine sensor. *J. Alloys Compd.* **716**, 96–105 (2017)
  25. L.-B. Kong, J.-W. Lang, M. Liu, Y.-C. Luo, L. Kang, Facile approach to prepare loose-packed cobalt hydroxide nano-flakes materials for electrochemical capacitors. *J. Power Sources* **194**(2), 1194–1201 (2009)
  26. N. Nadiah, F.S. Omar, A. Numan, Y. Mahipal, S. Ramesh, K. Ramesh, Influence of acrylic acid on ethylene carbonate/dimethyl carbonate based liquid electrolyte and its supercapacitor application. *Int. J. Hydrogen Energy* **42**(52), 30683–30690 (2017)
  27. T. Brousse, D. Bélanger, J.W. Long, To be or not to be pseudocapacitive? *J. Electrochem. Soc.* **162**(5), A5185–A5189 (2015)
  28. F.S. Omar, A. Numan, N. Duraisamy, S. Bashir, K. Ramesh, S. Ramesh, Ultrahigh capacitance of amorphous nickel phosphate for asymmetric supercapacitor applications. *RSC Adv.* **6**(80), 76298–76306 (2016)
  29. A.W. Anwar, A. Majeed, N. Iqbal, W. Ullah, A. Shuaib, U. Ilyas, F. Bibi, H.M. Rafique, Specific capacitance and cyclic stability of graphene based metal/metal oxide nanocomposites: a review. *J. Mater. Sci. Technol.* **31**(7), 699–707 (2015)
  30. J. Cherusseri, K.K. Kar, Hierarchically mesoporous carbon nanopetal based electrodes for flexible supercapacitors with super-long cyclic stability. *J. Mater. Chem. A* **3**(43), 21586–21598 (2015)
  31. N. Huang, H. Lim, C.H. Chia, M.A. Yarmo, M. Muhamad, Simple room-temperature preparation of high-yield large-area graphene oxide. *Int. J. Nanomed.* **6**, 3443 (2011)

**Publisher's Note** Springer Nature remains neutral with regard to jurisdictional claims in published maps and institutional affiliations.

Springer Nature or its licensor (e.g. a society or other partner) holds exclusive rights to this article under a publishing agreement with the author(s) or other rightsholder(s); author self-archiving of the accepted manuscript version of this article is solely governed by the terms of such publishing agreement and applicable law.